Journal of Rock Mechanics and Geotechnical Engineering 16 (2024) 379–392

Contents lists available at ScienceDirect

Journal of Rock Mechanics and Geotechnical Engineering

journal homepage: www.jrmge.cn

Full Length Article

On the calibration of a shear stress criterion for rock joints to represent the full stress-strain profile

Akram Deiminiat*, Jonathan D. Aubertin, Yannic Ethier

Department of Construction Engineering, École de Technologie Supérieure (ÉTS), Montréal, Canada

ARTICLE INFO

Article history:
Received 28 December 2022
Received in revised form
7 May 2023
Accepted 9 July 2023
Available online 6 November 2023

Keywords:
Full shear profile
Post-peak shear behavior
Rock joint
Joint roughness coefficient (*JRC*)
Axial stress-strain curve

ABSTRACT

Conventional numerical solutions developed to describe the geomechanical behavior of rock interfaces subjected to differential load emphasize peak and residual shear strengths. The detailed analysis of pre- and post-peak shear stress-displacement behavior is central to various time-dependent and dynamic rock mechanic problems such as rockbursts and structural instabilities in highly stressed conditions. The complete stress-displacement surface (CSDS) model was developed to describe analytically the pre- and post-peak behavior of rock interfaces under differential loads. Original formulations of the CSDS model required extensive curve-fitting iterations which limited its practical applicability and transparent integration into engineering tools. The present work proposes modifications to the CSDS model aimed at developing a comprehensive and modern calibration protocol to describe the complete shear stress-displacement behavior of rock interfaces under differential loads. The proposed update to the CSDS model incorporates the concept of mobilized shear strength to enhance the post-peak formulations. Barton's concepts of joint roughness coefficient (*JRC*) and joint compressive strength (*JCS*) are incorporated to facilitate empirical estimations for peak shear stress and normal closure relations. Triaxial/uniaxial compression test and direct shear test results are used to validate the updated model and exemplify the proposed calibration method. The results illustrate that the revised model successfully predicts the post-peak and complete axial stress–strain and shear stress–displacement curves for rock joints.

1. Introduction

Rock masses present networks of structural fractures (i.e. discontinuities and joints) which separate intact rock components. The mechanical properties of these interfaces greatly influence the behavior of rock masses. The potential for failure or rupture of the rock masses (e.g. slope failure, strain burst, rock falls) is largely attributed to shear strength of joint surfaces under load (Ladanyi and Archambault, 1969; Barton, 1982; Lee et al., 1990). A proper understanding of the shear behavior of structural interfaces is thus necessary to ensure safe and stable rock excavations.

Numerous criteria have been proposed to quantify shear strength of rock joints subjected to lateral and normal loads (e.g. Patton, 1966; Bandis et al., 1981; Saeb and Amadei, 1992; Grasselli and Egger, 2003; Barton, 2013; Zhang et al., 2014; Thirukumaran and Indraratna, 2016). These models predict the peak and/or residual shear strength of rock fractures based on superficial geometry (i.e. directional roughness) and rock geomechanical properties (e.g. compressive strength, elastic modulus) (Goodman, 1980). Limited considerations have been given to the practical quantification of total shear stress-strain profile of joints under loads. The pre- and post-peak strain profiles of loaded joints is of great importance in dynamic environments prone to time-dependent failure and rockburst events (Martin, 1993; Martin and Chandler, 1994; Fairhurst and Hudson, 1999; Simon, 1999; Simon et al., 2003; Khosravi, 2016; Khosravi and Simon, 2018). There are clear needs for a pragmatic and applicable numerical solution to describe the full shear stress-strain profile pre- and post-peak for rock interfaces under differential load.

Simon (1999) introduced a constitutive model to represent the complete stress displacement surface, the complete stress-displacement surface (CSDS) model. The model considers strains arising from compaction, shear, and normal deformation and it

* Corresponding author.
E-mail address: akram.deiminiat.1@ens.etsmtl.ca (A. Deiminiat).

Peer review under responsibility of Institute of Rock and Soil Mechanics, Chinese Academy of Sciences.

https://doi.org/10.1016/j.jrmge.2023.07.019

includes several model parameters that are needed to be obtained by triaxial compression and direct shear test data and extensive curve fitting (Simon, 1999; Simon et al., 2003). Subsequent works have been reported to develop and verify the proposed model (Deng et al., 2004; Tremblay, 2005; Tremblay et al., 2007; Khosravi, 2016). Notwithstanding, difficulties with the estimation of model parameters have never been removed, and the exemplified calibration process for CSDS remains opaque due to extensive curve fitting that diminishes the applicability of the model to practical realities of rock engineering. A rational for intuitive procedural calibration is required to develop CSDS further for holistic applications.

The goal of this work is to present a thorough stepwise procedure for the calibration of a complete shear stress-strain model. To this purpose, a modified version of the CSDS model is proposed to incorporate updated formulations for peak strength and normal closure, and account for mobilized shear strength. Validation for the updated model and the proposed calibration protocol is exemplified with experimental data taken from relevant literature. The results showcase the applicability of the model to represent the stress-strain behavior of rock interfaces during conventional direct shear and triaxial shear tests. This paper contributes a complete and readily applicable version of the CSDS model not published before, introduces an update to the model to reflect modern acknowledged precepts of field, presents a detailed and exhaustive calibration procedure to determine model parameters, showcases a multi-datasets validation of the model to showcase its applicability and the proposed calibration protocol, and demonstrates a number of application methods based on different shear testing programs (with direct and/or triaxial testing for post-peak and full profile representation).

2. Background

The shear behavior of rock interfaces can be characterized through direct or indirect experimental methods in laboratory settings. Direct shear testing and shear characterization in triaxial apparatus are described in ISRM (1989), ASTM D2664-04 (2004), ASTM D5607-16 (2016), ASTM D7012-23 (2023), (see also Franklin et al., 1974; Fardin, 2008; Tang and Wong, 2016; Liu et al., 2017; Day et al., 2017a, b; Packulak et al., 2018, 2022a, b). Fig. 1 depicts conceptually the stress-strain profile for a rock joint under shear loading. Similar features and profiles are expected from applying compression to a sample during direct shear and triaxial compression tests. The plot is characterized by near linear stress-strain correlation up to a maximum stress value associated with peak shear stress. Peak shear stress denotes the shearing and or crushing of superficial asperities, thus changing the roughness and potential for dilation. The post-peak behavior of rocks starts once the failure plane is created and the shear load decreases, eventually converging to a constant value and coined residual stress (Goodman et al., 1968; Goodman, 1976; Barton and Choubey, 1977; Martin and Chandler, 1994; Aubertin et al., 1998; Eberhardt et al., 1998).

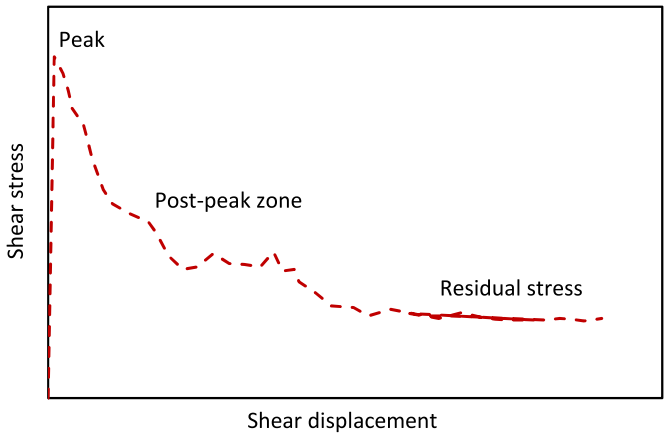

Fig. 1. Typical shear stress versus deformation curve for a rock joint under shear loading.

Joint deformation under normal load is quantified by its normal stiffness, K_n (MPa/mm) (Goodman et al., 1968). It can be measured by varying normal stress and measuring the corresponding strain normal to the discontinuity. The relation of normal stiffness with peak and residual shear displacement and maximum joint closure allows one to identify the contribution of joints to total displacement of a rock mass (Fotoohi, 1993). Joint shear behavior is highly affected by the change in normal stress (Goodman et al., 1968; Bandis, 1980; Fotoohi, 1993; Simon, 1999).

The shear behavior of rock joints is heavily dependent upon external factors (e.g. shear load direction, span, stress profile) and the geomechanical characteristics of the rock and its interfaces (e.g. morphology of discontinuities, mechanical strength, elastic properties, weathering conditions). Extensive studies have parametrized the influence of intrinsic and external factors on the behavior of rock joints under differential loads (see for example Goodman et al., 1968; Barton, 1973; Bandis, 1980; Simon, 1999; Grasselli, 2001; Fardin et al., 2001, 2004; Simon et al., 2003; Fardin, 2008; Sanei et al., 2015a; Tang and Wong, 2016; Khosravi, 2016; Yang et al., 2016; Liu et al., 2017; Niktabar et al., 2017; Li et al., 2022; Wang et al., 2022).

Various criteria have been proposed over the years to quantify peak shear strength of rock joints with respect to the applied normal load by accounting for both external and intrinsic factors. Patton (1966) proposed a bilinear model by incorporating surface roughness (i.e. asperities) to Mohr-coulomb failure criterion. Ladanyi and Archambault (1969) developed a more comprehensive failure model, the LADAR model, based on actual shear contact surfaces and inclination angle, and applicable to different irregular joint surfaces. Since then, several failure criteria have been developed by implementing roughness parametrization (e.g. Barton, 1973; Barton and Choubey, 1977; Bandis et al., 1981; Barton, 1982; Fortin et al., 1988; Amadei and Saeb, 1990; Saeb and Amadei, 1992; Huang et al., 1993; Haberfield and Johnston, 1994; Homand et al., 2001).

The joint roughness coefficient (*JRC*) proposed by Barton and Choubey (1977) progressively became a standard index of reference to represent joint surface geometry (ISRM, 1978). The subjective nature of this index has been discussed at length by various authors (Grasselli, 2001; Sanei et al., 2015b; Khosravi, 2016; Li et al., 2022). Researchers proposed correlations between objective roughness parameters (e.g. fractal dimension, D; roughness profile index, R_p; surface parameter, Z_2) and *JRC* (Yang et al., 2001; Jang et al., 2006; Kim et al., 2009; Tatone and Grasselli, 2010). Grasselli (2001) used apparent dip angle of joint surface with respect to the shear direction to find a three-dimensional (3D) criterion for the estimation of peak shear strength of the entire rock joint surface. This method was followed by many researchers (Grasselli et al., 2002; Grasselli and Egger, 2003; Xia et al., 2014; Tang and Wong, 2016; Yang et al., 2016; Liu et al., 2017; Tian et al., 2018; Magsipoc et al., 2020).

Models based on mobilized shear strength have also been proposed to predict the post-peak shear strength (e.g. Bandis et al., 1983; Asadollahi, 2009). Simon (1999) developed the CSDS model to describe the post-peak shear behavior for rock joints in the context of describing rockburst-prone rock mass conditions. The

Table 1
Summary of the updated CSDS formulation.

Shear stress–shear displacement	Normal displacement–shear displacement	Axial strain on the pre peak stress–strain curve
$F(u) = \tau = a + b\exp(-cu) - d\exp(-eu)$	$V = \beta_1 - \beta_2\exp(-\beta_3 u)$	$\varepsilon_{prepeak} = \varepsilon + \frac{\Delta u\cos\beta}{L} + \frac{\Delta V\sin\beta}{L} + \frac{\Delta\sigma_1}{E}$
$a \approx \tau_r$	$\beta_1 = u_r\tan[JRC_m\log_{10}(\sigma_c/\sigma_n)]$	
$a + b = d$	$JRC_m = JRC_p(u/u_p)^{-0.381}$	
$c \approx 5/u_r$	$JRC_p = \frac{\arctan(\tau_p/\sigma_n) - \varphi_b}{\log_{10}(JCS/\sigma_n)}$	
$d = \frac{\tau_p - \tau_r\left[1 - \exp\left(-\frac{5u_p}{u_r}\right)\right]}{\exp\left(-\frac{5u_p}{u_r}\right) - \exp(-eu_p)}$	$\beta_2 = \beta_1 - \frac{\sigma_n V_m}{K_{ni}V_m - \sigma_n}$	
$\frac{deu_r}{5(d-\tau_r)} - \exp[u_p(e - 5/u_r)] = 0$	$V_m = 8.57(JCS/a_j)^{-0.68}$	
$\tau_p = \sigma_n\tan[JRC_p\log_{10}(JCS/\sigma_n) + \varphi_b]$	$K_{ni} = 0.02(JCS/a_j) + 1.75JRC_p - 7.15$	
$u_p = 0.0077L^{0.45}(\sigma_n/JCS)^{0.34}\cos[JRC_p\log_{10}(JCS/\sigma_n)]$	$a_j = \frac{JRC_p}{5}(0.2\sigma_c/JCS - 0.1)$	
$\tau_r = \sigma_n\tan\varphi_r$	$\beta_3 = 1.5/u_r$	

Note: a, b, c, d, e, β_1, β_2 and β_3 are the model parameters for CSDS; τ, τ_{peak} and τ_r are the shear stress, shear stress at peak (maximum shear stress), and residual shear stress, respectively; σ_n, σ_c and σ_1 are the normal stress, uniaxial compressive strength and main axial stress, respectively; u_p and u_r are the peak and residual displacements, respectively and correspond with t_{peak} and t_r; φ_b and φ_r are the basic friction angle and residual friction angle, respectively; V_m, k_{ni}, a_j, JRC_p, JRC_m, JCS and L are the maximum closure, initial normal stiffness, initial joint aperture, peak joint roughness coefficient, mobilized joint roughness coefficient, joint compressive strength and specimen length, respectively; ε, $\varepsilon_{prepeak}$ and β are the axial strain, pre-peak strain and shear plane angle, respectively.

model was refined and adapted to predict the hydromechanical behavior of rock joints by Tremblay et al. (2007).

The present study aims to adapt the CSDS model by incorporating peak shear strength, mobilized joint roughness and normal closure models. In addition to provide a simple procedural method for calibration, the adapted model can describe full shear behavior of rocks from triaxial/axial compression tests with or without direct shear tests. In this article, the CSDS model is first introduced. Certain and proven formulae that are used to modify the models' calibration method are presented next. The step-by-step CSDS model calibration proposed in this study is then presented and exemplified by using a series of data sets taken from the literature.

3. Complete stress displacement surface (CSDS) model

The CSDS model implements an exponential function to describe the relationship between shear stress τ (MPa) and shear displacement u (mm) (Simon, 1999):

$$F(u) = \tau = a + b\exp(-cu) - d\exp(-eu) \tag{1}$$

where a, b, c, d and e are the model parameters with the condition of a, b, c, d, $e > 0$ and $c < e$.

Boundary conditions for the model formulation help derive values of model parameters. Under initial testing conditions (i.e. $u = 0$), there is no deformation and no corresponding load. Therefore, we have

$$a + b = d \tag{2}$$

At large displacement (i.e. $u \gg 0$), it is intuited that shear stress has reached residual state τ_r (MPa). The two exponential components approach 0, thus we have

$$F(u \gg 0) = \tau_r \approx a \tag{3}$$

When shear deformation has reached residual conditions (i.e. $u = u_r$), then it follows that

$$F(u_r) = a + b\exp(-cu_r) - d\exp(-eu_r) = \tau_r \tag{4}$$

Then, we have

$$b\exp(-cu_r) - d\exp(-eu_r) = \tau_r - a = 0 \tag{5}$$

Based on extensive experimental data, Simon et al. (2003) proposed to approximate exponential component of $-cu_r$ as 0.07, i.e.

$$\exp(-cu_r) \approx 0.07 \tag{6}$$

$$\therefore c \approx 5/u_r \tag{7}$$

Since shear stress peaks at $u = u_p$, the derivative of Eq. (1) with $u = u_p$ must equal zero, i.e.

$$\left.\frac{\partial F(u)}{\partial(u)}\right|_{u=u_p} = -5/u_r(d - \tau_r)\exp(-5u_p/u_r) + de\exp(-eu_p) = 0 \tag{8}$$

$$\therefore \frac{deu_r}{5(d - t_r)} - \exp[u_p(e - 5/u_r)] = 0 \tag{9}$$

At peak displacement, $F(u_p) = \tau_p$, thus we have

$$\tau_p - \tau_r[1 - \exp(-5u_p/u_r)] - d[\exp(-5u_p/u_r) - \exp(-eu_p)] = 0 \tag{10}$$

Parameter d is isolated in Eq. (10) to yield

$$d = \frac{\tau_p - \tau_r[1 - \exp(-5u_p/u_r)]}{\exp(-5u_p/u_r) - \exp(-eu_p)} \tag{11}$$

where τ_p and τ_r are the peak and residual strengths, respectively (MPa); and u_p and u_r are the displacements at the peak and residual shear stresses, respectively (mm).

Based on Eqs. (2)–(11), the model parameters can be derived from physical measurements obtained in the conventional laboratory experiments.

An exponential function was proposed by Simon (1999) to describe the normal displacement (V) versus shear displacement (u) relationship:

$$V = \beta_1 - \beta_2 \exp(-\beta_3 u) \tag{12}$$

where β_1, β_2 and β_3 are the model parameters. The procedure for determining these parameters is described below.

It goes from the above equation that for $u = 0$, $V \equiv \beta_1 - \beta_2$. β_2 is derived by following the relationship between normal load and displacement described by Bandis et al. (1983):

$$V = \frac{\sigma_n V_m}{K_{ni} V_m - \sigma_n} \tag{13}$$

where σ_n is the normal stress applied to rock joint (MPa), V_m is the maximum closure of the rock joint (mm), and k_{ni} is the initial normal stiffness (MPa/mm). It follows that

$$\beta_2 = \beta_1 - \frac{\sigma_n V_m}{K_{ni} V_m - \sigma_n} \tag{14}$$

At $u \gg 0$, $V = \beta_1$ and $u = u_r$.

By using the model proposed by Goodman and St John (1977) (Eq. (15)), one can obtain β_1 using Eq. (16).

$$V = u_r (1 - \sigma_n/\sigma_c)^{k_2} \tan i_0 + \frac{\sigma_n V_m}{K_{ni} V_m - \sigma_n} \tag{15}$$

$$\beta_1 = u_r (1 - \sigma_n/\sigma_c)^{k_2} \tan i_0 + \frac{\sigma_n V_m}{K_{ni} V_m - \sigma_n} \tag{16}$$

where σ_c is the compressive strength of rock (MPa), $k_2 = 4$, and i_0 is the initial asperity angle (°).

Based on many experimental data taken by Simon (1999) from the literature, it was found that the last parameter, β_3, may be related to the residual displacement (u_r) as follows:

$$\beta_3 \cong 1.5/u_r \tag{17}$$

4. Proposed modification to the CSDS model

A series of modifications is proposed to improve CSDS' ease of calibration. These changes provide specific and proven formulations for certain model parameters that may otherwise require extensive curve fitting. The modifications and rationale for empirical justifications are described below. A compiled summary of the updated CSDS formulation is provided in Table 1.

4.1. Normal closure model after Bandis et al. (1983)

Rock joint deformability can be described by the properties of stress-deformation curve (Goodman et al., 1968; Fotoohi, 1993). Exponential equations have been suggested by Bandis et al. (1983) to determine the maximum closure and initial normal stiffness as follows:

$$V_m = 8.57 (JCS/a_j)^{-0.68} \tag{18}$$

$$K_{ni} = 0.02 (JCS / a_j) + 1.75 JRC_p - 7.15 \tag{19}$$

where a_j is the initial joint aperture (mm) and it can be obtained by

$$a_j = \frac{JRC_p}{5} (0.2\sigma_c / JCS - 0.1) \tag{20}$$

where σ_c is the uniaxial compressive strength (MPa) and JCS is the joint compressive strength (MPa). Eqs. (18)–(20) are proposed to facilitate the determination of β_1 and β_2 in Eqs. (14) and (16).

4.2. Mobilized shear strength after Barton (1982) and Asadollahi (2009)

Barton (1982) modified the peak shear strength model of Barton-Bandis to take the stress dependency of shear strength into account. The modified model considers the progressive degradation of joint roughness during the shear process, mobilized joint roughness coefficient (JRC_m). The failure model is then proposed as follows:

$$\tau = \sigma_n \tan[JRC_m \log_{10}(JCS / \sigma_n) + \varphi_r] \tag{21}$$

$$JRC_m = \frac{\arctan(\tau_m/\sigma_n) - \varphi_r}{\log_{10}(JCS/\sigma_n)} \tag{22}$$

where τ is the mobilized shear stress (MPa) and φ_r is the residual friction angle (°).

From Eq. (22), one can determine the mobilized JRC and joint roughness changes during shearing. Also, Barton (1982) described a dimensionless relationship between JRC_m/JRC_p and u/u_p in a table, called Barton table. Once u_p and JRC_p are obtained from experimental data, JRC_m and shear strength can be determined. However, this method could not obtain a complete post-peak curve, particularly precise residual shear strength (Asadollahi and Tonon, 2010; Khosravi and Simon, 2018).

Asadollahi (2009) modified Barton's model for the peak displacement and the dimensionless relationship between JRC and shear displacement to predict the shear strength more precisely:

$$\frac{JRC_m}{JRC_p} = \left(\frac{u}{u_p}\right)^{-0.381} \tag{23}$$

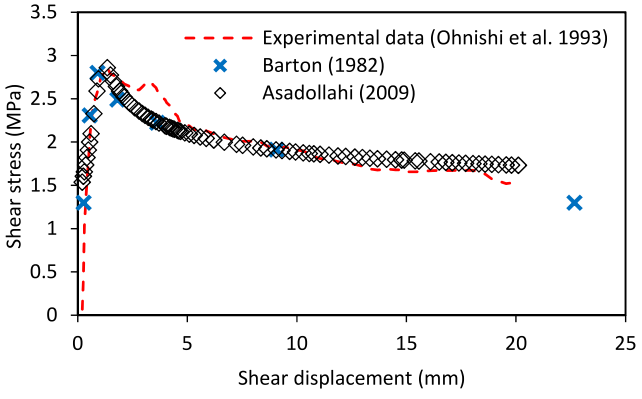

Fig. 2. A comparison between the post-peak shear behavior of rock joint predicted by Barton and Asadollahi models and experimental data obtained by Ohnishi et al. (1993).

$$u_p = 0.0077L^{0.45}(\sigma_n/JCS)^{0.34}\cos\left[JRC_p \log_{10}(JCS/\sigma_n)\right] \quad (24)$$

where L is the specimen length (m).

Asadollahi and Tonon (2010) validated proposed models by using 365 direct shear test data taken from the literature in which the *JRC* ranged between 0 and 20 with normal distribution. The average ratio of predicted u_p over measured u_p was reported as 1.11 with standard deviation of 0.76 and the average ratio of predicted $JRC_{mobilised}$ to measured $JRC_{mobilised}$ was 1.19 with standard deviation of 0.92.

Furthermore, Fig. 2 shows the application of Barton and Asadollahi models for the direct shear tests on a cement mortar with irregular surface, which are taken from Ohnishi et al. (1993). As shown, the post-peak shear stress obtained by Asadollahi (2009) predicts quite well the experimental curve whereas the curve obtained by Barton model decreases as the shear displacement increases. This observation may be due to the 0-value defined in Barton's table for JRC_m/JRC_p when $JRC_p > 5$ and $u/u_p = 25$. Hence, the model proposed by Asadollahi (2009) is used in this study to determine the JRC_m and u_p.

Since the JRC_m is obtained from Eq. (23) for all the data points on the experimental curve, the CSDS model parameter, β_1, is suggested to be calculated as follows:

$$\beta_1 = u_r \tan[JRC_m \log_{10}(\sigma_c/\sigma_n)] \quad (25)$$

4.3. Peak shear strength criterion after Barton and Choubey (1977)

Barton and Choubey (1977) proposed the commonly acknowledged peak shear strength criterion based on roughness conditions (represented by *JRC*) and joint compressive strength *JCS*:

$$\tau_p = \sigma_n \tan\left[JRC_p \log_{10}(JCS/\sigma_n) + \varphi_b\right] \quad (26)$$

JRC_p can be obtained directly by profiling rock joint specimens using profilometer. Ten typical roughness profiles given by Barton (1973) for *JRC* ranging from 0 to 20 can then be used. The joint roughness coefficient can also be determined by the back-calculation of Eq. (26), when other parameters are available from the experimental data. In this equation, *JCS* can be determined by Schmidt hammer tests. Alternatively, *JCS* can be estimated as the unconfined compressive strength (σ_c) of the intact rock for fresh joints and $\sigma_c/4$ for highly weathered rocks (Barton, 1973; Barton and Choubey, 1977). Additional information on *JCS* measurements, empirical estimates and complementary techniques for the application of *JRC* and *JCS* can be found in Barton (2013), Zheng and Qi (2016), Liu et al. (2017), and Tang et al. (2021). For further analyses in this work, the peak value of shear strength predicted from Eq. (1) and/or measured by experimental work is considered equal to the peak shear strength obtained by Eq. (26). The Barton model is suggested here because of easy application of the model in industry and general trust in the calculations based on *JRC* and *JCS*.

5. CSDS model calibration

This section describes the updated calibration method of CSDS model for post-peak and full shear behavior of rock discontinuities with the use of triaxial compression test with/without direct shear test data. The model calibration includes some general steps remained from Simon et al. (2003) and detailed steps proposed in this study. The model is then exemplified in the next section.

5.1. Post-peak shear stress-displacement curves with triaxial/uniaxial compression tests

The CSDS model can be applied to describe traditional direct shear testing detailed by ISRM (1978) and ASTM D5607-16 (2016). As reported by Simon et al. (2003), the relevant experimental parameters, i.e. φ_b, τ_p, τ_r, u_p, u_r, *JCS* and elastic modulus (E) are first obtained from traditional interpretation of triaxial and uniaxial testing experimental process. Then, the model parameters such as a, b, c, d and e are determined through Eqs. (2)–(11). The following procedural workflow, proposed in this study, is subsequently used to calibrate the model.

(1) JRC_p is obtained by back calculation from Eq. (26).
(2) For all the post-peak data points on triaxial stress–strain curve, the ratios of u/u_p (or $\varepsilon/\varepsilon_p$) are calculated and added to Eq. (23) to determine JRC_m.
(3) Values for a_j, V_m and K_{ni} are directly calculated by Eqs. (18)–(20) to ensure that the influence of joint deformation is considered in the analyses.
(4) By using the obtained parameters and experimental data, the CSDS model parameters β_1, β_2 and β_3 can be determined through Eqs. (14), (17) and (25), respectively.
(5) The variation of axial strain on the post-peak stress–strain curve is a function of several parameters (Simon et al., 2003):

$$\varepsilon = \varepsilon_p + \frac{\Delta u\cos\beta}{L} - \frac{\Delta V\sin\beta}{L} + \frac{\Delta\sigma_1}{E} \quad (27)$$

where ε is the axial strain, ε_p is the peak strain, Δu is the difference in shear displacement (mm), ΔV is the difference in normal displacement (mm), $\Delta\sigma_1$ is the difference in principal axial stress (MPa), L is the initial sample length (mm), E is the elastic modulus of rock (MPa), and β is the shear plane angle (°).

For each data on the post-peak stress-strain curve, the peak and elastic strains are subtracted from Eq. (27), thus we have

$$\varepsilon^* = \varepsilon - \varepsilon_p - \Delta\sigma_1/E \quad (28)$$

where ε^* is the modified post-peak strain.

At the 1st point, $\Delta V_1 = V_1 = 0$. Eq. (27) becomes

$$\Delta u_1 = (\varepsilon_1 - \varepsilon_p - \Delta\sigma_{1,1}/E)(L/\cos\beta), \Delta u_1 = u_1 \quad (29)$$

At the 2nd point, from Eq. (12), we have

$$V_2 = \beta_1 - \beta_2 \exp(-\beta_3 u_1), \Delta V_2 = V_2 - V_1$$

From Eq. (27), we have

$$\Delta u_2 = \left(\varepsilon_2 - \varepsilon_p - \Delta\sigma_{1,2}\Big/ E + \frac{\Delta V_2 \sin\beta}{L}\right)(L/\cos\beta), u_2 = \Delta u_2 + u_1 \quad (30)$$

The same procedure is repeated for all subsequent datapoints on the post-peak stress–strain curve. The calculated values of Δu and model parameters are used in Eq. (1) to determine the shear stress.

5.2. Full shear stress-displacement curves with triaxial compression tests, with/without direct shear tests

When direct shear tests are available, the model properties (e.g. τ_p, τ_r, u_p, u_r) are directly derived through the shear curves in order

to determine the model parameters such as a, b, c, d and e. Once the model parameters are determined, Steps (1)–(5) in the preceding section are carried out by using the axial stress and strains obtained from triaxial compression tests. It should be noted that, since the complete shear displacement is required in this section, the values of u obtained by following Step (5) are used in Eq. (1) for estimating the shear stress.

An alternative method is proposed in this study to approximate the calibration process in the absence of direct shear test data. In this method, the measured joint roughness coefficient and Barton model can be used to determine peak shear strength (τ_p). The Coulomb criterion without cohesion is used to obtain the residual friction angle:

$$\tau_r = \sigma_n \tan(\varphi_r) \tag{31}$$

The φ_r is thus used to calculate the residual shear strength under the imposed normal load(s). The corresponding residual displacement for τ_r is denoted by u_r that can be determined using curve fitting and back calculation of CSDS model. Since *JCS* and JRC_p are known, Eq. (24) may be utilised to determine u_p. When direct shear test does not reach the actual residual shear stress and subsequently residual shear displacement, the residual shear data can be obtained by the alternative method.

5.3. Full shear stress-displacement curves with direct shear tests

When the direct shear test data and mechanical properties of rock (e.g. φ_b, *JCS* (or σ_c), E) are available, the model properties are directly extracted from shear curves to determine the model parameters such as a, b, c, d and e using Eqs. (2)–(11). Subsequently, the shear stress can be calculated. Depending on the direct shear machine and applied normal load, direct shear test may not reach the actual residual shear stress and subsequently residual shear displacement. The residual shear stress can thus be obtained by using Eq. (31), and u_r can be back-calculated with the CSDS model (Eq. (1)) and curve fitting.

Concerning the normal displacement–shear displacement curves, the method suggested in this study is followed. The mobilized *JRC* values are first obtained from Eq. (22). Then, the normal closure parameters (e.g. a_j, V_m, K_{ni}) are determined to be able to calculate the model parameters β_1, β_2 and β_3 and normal displacement from Eqs. ((12), (14), (17) and (25). Since the suggested formulae for the estimations of β_1 and β_2 are based on normal stress, only one value is obtained for each parameter.

5.4. Full axial stress-strain curves with triaxial/uniaxial compression tests

The proposed method for post-peak stress–strain estimation resembles the method initiated by Simon et al. (2003), with some modifications that are highlighted below along with the proposed method for pre-peak curve.

The model parameters must first be determined from triaxial compression tests using the procedure outlined in Section 5.1. Once the model parameters are obtained, the following steps must be taken:

(1) For the data on stress-strain curve, the shear and normal stresses are calculated by the following formulae:

$$\sigma_n = \frac{1}{2}(\sigma_1 + \sigma_3) - \frac{1}{2}(\sigma_1 - \sigma_3)\cos(2\beta) \tag{32}$$

$$\tau = \frac{1}{2}(\sigma_1 - \sigma_3)\sin(2\beta) \tag{33}$$

where σ_1 is the major principal stress (MPa), and σ_3 is the minor principal stress (MPa).

(2) For the corresponding values of shear stress, the shear displacement (u) can be computed through Eq. (1) and the application of a linear solver available in common computation tools (e.g. MS Excel solver, see the detailed application in Li et al. (2000)). There are two values for u, which should be noted. The value larger than the peak displacement (u_p) should be used for the current analysis.
(3) By using the predicted u values, obtained β_1 (by using Eq. (25) suggested in this study), β_2 and β_3 and Eq. (12), the normal displacement (V) can be calculated.
(4) The axial strain can then be estimated by adding the predicted shear and normal displacements into Eq. (27). For the pre peak profile, since the volume change is positive before shear stress reaches to the peak (Goodman, 1976; Martin and Chandler, 1994), the normal displacement should be obtained using Eq. (34). The axial strain can thus be predicted with Eq. (35).

$$V = -[\beta_1 - \beta_2 \exp(-\beta_3 u)] \tag{34}$$

$$\varepsilon_{pre-peak} = \varepsilon + \frac{\Delta u \cos\beta}{L} - \frac{\Delta V \sin\beta}{L} + \frac{\Delta\sigma_1}{E} \tag{35}$$

where $\varepsilon_{pre\text{-}peak}$ is the axial strain before peak.

6. Validation of updated CSDS

6.1. Scope of validation work carried

The next sections showcase the use and application of the CSDS model in its updated form, and the calibration method proposed in the previous sections. The model is applied to different experimental settings commonly encountered with laboratory characterization for shear testing. Validation is carried out for test programs with triaxial and/or direct shear tests for post-peak and full profile representations. The validation work was carried out on direct shear and triaxial compression tests originally presented in Price (1979), Ohnishi et al. (1993), Arzúa and Alejano (2013), Khosravi and Simon (2018) and Khosravi (2016). These data sets include both direct and triaxial shear test results with servo-controlled machine for the full pre- and post-peak profile.

6.2. Post-peak shear stress-displacement estimation with triaxial compression tests

This section exemplifies the application of the updated model to describe post-peak shear stress–displacement curve. The curves predicted by the original CSDS model (Simon et al., 2003) are also included in the results to showcase the validity and evolution of the model. The experimental data on sandstone were taken from Price (1979) for different confining pressures.

Table 2
Rock properties and CSDS model properties that are obtained by Simon et al. (2003).

σ_3 (MPa)	B^a (°)	E^a (GPa)	u_p (mm)	u_r (mm)	i_o (°)	K_{ni} (MPa/mm)	V_m (mm)	$\sigma_T{}^a$ (MPa)	$S_o{}^a$ (MPa)	$\varphi_0{}^a$ (°)	φ_r (°)
0	35	18	0.008	8	25	−1000	1	95	16	46	44
4	33	18	0.008	8	25	−1000	1	95	16	46	44
7	33	18	0.008	8	25	−1000	1	95	16	46	44
14	30	18	0.008	8	25	−1000	1	95	16	46	44

[a] Parameters are taken from Price (1979).

Table 2 shows the rock properties and CSDS model properties obtained by Simon et al. (2003) for four tests, and Table 3 gives the model properties that are determined by the updated model for different confining pressures. Fig. 3 illustrates a comparison of post-peak shear stress-displacement curves obtained by this study and those taken from Simon et al. (2003). The results reveal that the new model always calibrates well the residual shear stress. It is perfectly illustrated in Fig. 3c and d. In addition, it is noted from Table 2 that the k_{ni} and V_m values obtained from curve fitting are seemingly arbitrary and/or subjective to the user. The updated method presents a systematic solution to derive these values as showcased in Table 3.

To further validate the proposed model, the triaxial compression tests on basalt (BAS) and microgabbro (MG) reported by Khosravi (2016) and tests on granitic rock (Blanco Mera) reported by Arzúa and Alejano (2013) are used. Tables 4 and 5 show the rock properties taken from the literature and the model properties obtained in this study for BAS and MG and Blanco Mera, respectively.

Since no representative curves predicted by the original CSDS model could be found in Arzúa and Alejano (2013) and Khosravi (2016), Figs. 4 and 5 illustrates a comparison between the original curves reported by these studies and the post-peak shear behavior of the tested rocks obtained in this work. It is shown that the post-peak shear curves of all tests accurately represent the original curves. Similar observation can be made from Fig. 5 between the curves obtained in this work and the original curves obtained by Arzúa and Alejano (2013). It is questionable, however, whether the predicted shear stress–displacement curves from triaxial compression testing can also represent the curves obtained from direct shear tests. This issue is addressed in the following section.

6.3. Full shear behavior estimation with triaxial compression tests, with/without direct shear tests

To evaluate the accuracy of the proposed method for the full shear stress–displacement curve, two series of laboratory test results are used. One series are the results of triaxial compression tests on BAS-29 that are reported by Khosravi (2016). Another series are direct shear test data of the same rock obtained by Khosravi and Simon (2018) at normal loads of 3 MPa, 5 MPa and 8 MPa. Table 6 shows the rock characteristics used for the analysis. Table 7 shows the direct shear test data from Khosravi and Simon (2018), whereas Table 8 shows the model properties obtained in this study by the updated model.

The full shear curves of the tested rock are shown in Fig. 6 for different methods at three normal loads. A comparison between the predicted and original curves reveals that the proposed model correctly predicts the pre- and post-peak shear stress–displacement curves at varying normal loads. The similar conclusion can be given by comparing the model properties presented in Tables 7 and 8 However, significant differences are observed, when comparing the u_p and u_r values obtained with triaxial compression test data (see Table 4) to those obtained with direct shear test data of the same rock (see Table 8), indicating that direct shear tests are required to obtain reliable full shear stress-displacement curves for a rock joint.

The experimental data of BAS-29 are used again to further demonstrate how the full shear curves can be obtained without direct shear test data. In Table 9, one can see the model properties obtained by using the alternative method.

The full shear stress–displacement curves obtained without the use of direct shear tests are illustrated in Fig. 6 for different normal loads. As seen, the curves obtained by applying the normal stresses of 5 MPa and 8 MPa are successfully predicted. However, the predicted post-peak zone in Fig. 6c seems to have a difference of 0.5 to the residual shear stresses obtained with the use of direct shear tests. This may be shown further by comparing the data presented in Tables 7–9 for the three normal loads. The model properties in Table 9, which correspond to the predicted curves without direct shear tests, are quite close to those in Tables 7 and 8 These results tend to show that when direct shear tests are not available, the alternative method may be used to describe the full shear stress–displacement curve. Nevertheless, more works with the use of experimental data of different materials under different normal loads are required to further validate the alternative method.

6.4. Full shear stress-displacement and normal-shear displacement curves estimation with direct shear tests

The accuracy of the proposed method for the full shear stress–displacement curves when only direct shear tests are available is studied by using the experimental data of cement mortar with irregular surface taken from Ohnishi et al. (1993). Table 10 indicates the characteristics of the rock sample and the CSDS model properties obtained in this study. Fig. 7 shows the full shear stress-displacement and normal-shear displacement curves obtained from direct shear tests and those obtained by the proposed method. The curves obtained in this study exhibit the same trends as those of the original curves. For the experimental data, the shear stress–displacement curve tends to not behave as a perfect curve. This can be due to the rock joint deformation and rock asperities.

6.5. Full and post peak axial stress–strain curves estimation with triaxial compression tests

The triaxial compression test results of sandstone reported by Price (1979) are used to obtain the post peak axial stress–strain curves using the updated CSDS model. The rock properties taken from Price (1979), the model properties obtained by the original CSDS model and those obtained by the updated CSDS model in this study are previously reported in Tables 2 and 3, respectively.

Fig. 8 compares the experimental post peak stress–strain curves and those obtained by Simon et al. (2003) and this study. As seen, the updated model always results in curves that perfectly fit the original curves. The curves obtained by the original model do not show the residual stress. In all the curves, the post peak stress decreases when the axial strain increases. Unlike, the predicted curves in this study show the same trend as those of experimental data. This observation may be explained by including the mobilized

Table 3
Rock properties taken from Price (1979) and the model properties obtained in this study.

σ_3 (MPa)	B^a (°)	E^a (GPa)	u_p (mm)	u_r (mm)	JRC_p	K_{ni} (MPa/mm)	V_m (mm)	$\sigma_T{}^a$ (MPa)	$S_o{}^a$ (MPa)	$\varphi_0{}^a$ (°)
0	35	18	0.008	4.2	22.6	36.6	0.23	95	16	46
4	33	18	0.008	8	25	41.1	0.24	95	16	46
7	33	18	0.006	4.5	38.8	62.1	0.33	95	16	46
14	30	18	0.008	8	44.9	72.9	0.36	95	16	46

[a] Rock properties.

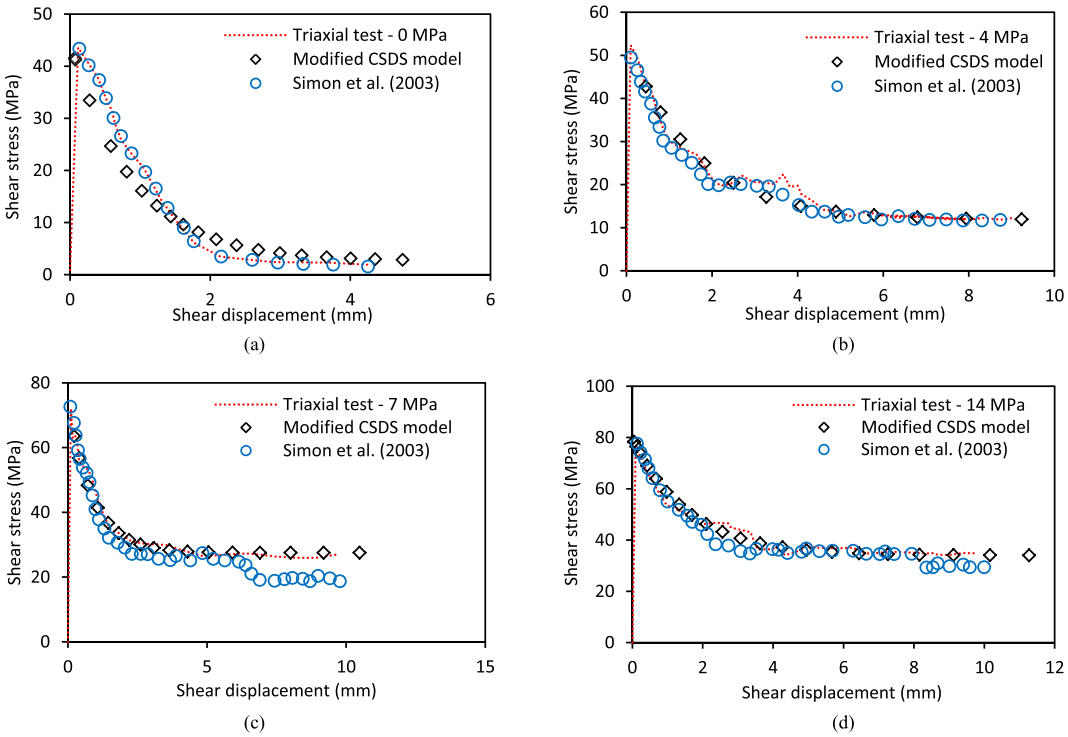

Fig. 3. Comparison of the post-peak shear stress–displacement curves obtained by the updated model with those obtained by Simon et al. (2003) for triaxial compression tests on sandstone with confining pressures of (a) 0 MPa, (b) 4 MPa, (c) 7 MPa and (d) 14 MPa. The experimental data are taken from Price (1979).

Table 4
Rock properties taken from Khosravi (2016), and the model properties obtained in this study for basalt (BAS) and microgabbro (MG).

Sample	σ_3 (MPa)	B^a (°)	E^a (GPa)	u_p (mm)	u_r (mm)	JRC	K_{ni} (MPa/mm)	V_m (mm)	$\sigma_T{}^a$ (MPa)	$S_o{}^a$ (MPa)	$\varphi_0{}^a$ (°)	φ_r (°)	i_0 (°)
BAS-23	20	22	45.4	0.015	1.1	10.96	37.6	0.07	280	33	53	34	19
BAS-29	24	17	45.4	0.002	1.3	22.6	44.9	0.1	280	33	53	43	34.7
MG-17	24	24	39	0.007	0.5	14.7	30.85	0.11	180	27	48	42	32.7
MG-19	15	25.5	39	0.02	1.12	19.4	36.04	0.13	180	27	52	49	37

[a] Rock properties.

Table 5
Rock properties taken from Arzúa and Alejano (2013), and the model properties obtained in this study.

σ_3 (MPa)	B (°)	E^a (GPa)	u_p (mm)	u_r (mm)	JRC	K_{ni} (MPa/mm)	V_m (mm)	$\sigma_T{}^a$ (MPa)	$S_o{}^a$ (MPa)	$\varphi_0{}^a$ (°)	φ_r (°)	i_0 (°)
4	24.3	22.61	0.045	2.53	31	48.9	0.39	57.8	8	46	52.4	38.7
12	14.2	48.84	0.07	2.5	38.2	63.1	0.26	126.7	16.8	46	48.5	49.5

[a] Rock properties.

roughness and joint normal closure model into the analyses after peak.

The full axial stress–strain curves can also be described by the updated model for rock joints. To this purpose, the triaxial compression tests on BAS and MG rocks reported by Khosravi (2016) are used. The model properties obtained in this study for BAS and MG are presented in Table 4. Table 11 shows the rock properties and model properties obtained by Khosravi (2016) using the original CSDS model. According to the data in Table 11, similar peak displacement equal to 0.005 mm was obtained for different samples and different confining pressures. The influences of confining pressure and rock properties on the peak and residual displacements are ignored in the method used by the authors. Furthermore, the values of k_{ni} and V_m are not published, and it is

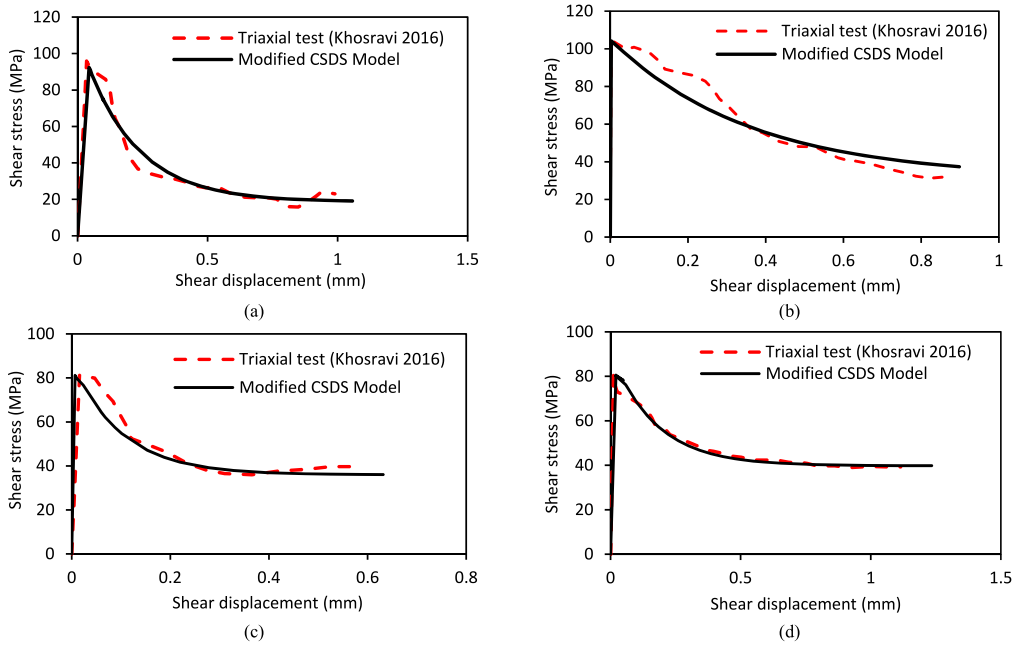

Fig. 4. Post-peak shear stress–displacement curves obtained by the modified model, and the original curves reported by Khosravi (2016) for (a) BAS-23, (b) BAS-29, (c) MG-17, and (d) MG-19.

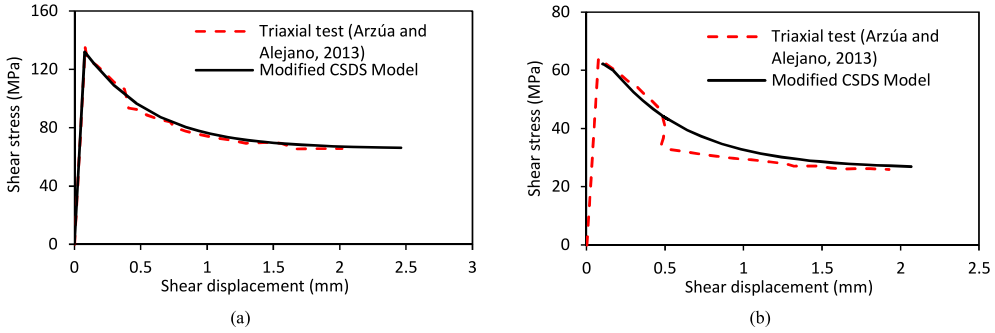

Fig. 5. A comparison of the post-peak shear stress–displacement curves obtained by the modified model to the original curves reported by Arzúa and Alejano (2013) for (a) $\sigma_3 = 4$ MPa and (b) $\sigma_3 = 12$ MPa.

unclear how the normal displacement parameters are obtained by the CSDS model.

Fig. 9 illustrates the experimental and predicted full stress-strain curves for different rocks. Comparisons of the original curves with the curves obtained by Khosravi (2016) and this study show that the updated model provides more accurate results for the full stress curves of four rocks, notably for the post-peak zone and residual stress.

Similarly, the triaxial compression test results of granitic rock, Blanco Mera, reported by Arzúa and Alejano (2013) are used to further evaluate the updated model. The rock joint properties taken from literature as well as the model properties obtained in this study are presented in Table 12. Fig. 10 compares the predicted full stress–strain curves with the original curves for confining pressures of (a) 4 MPa and (b) 12 MPa. The complete profiles between axial stress and strain precisely fit the experimental curves. These results confirm once again the validity of the proposed model.

7. Discussion

The present work aimed to contribute the field of rock engineering with a complete shear stress-displacement model developed for holistic applications and with a comprehensive calibration method. To achieve this development, an updated version of the CSDS model was presented to address certain practical limitations of the original formulations. The proposed model considers direct estimation of normal closure parameters (e.g. V_m and K_{ni}) and implements mobilized joint roughness coefficient for peak and residual approximations. A procedural step-by-step protocol was presented to guide calibration efforts using laboratory experiment data from direct shear tests and triaxial shear tests.

Validations carried on various experimental data sets demonstrate that the suggested method improved the calibration of the CSDS model for the post-peak and full shear behavior of rock joints. Additional work shall be carried in the future to further validate the application of the model to other data sets, other types of rocks, and other testing configurations. Deng et al. (2006) presented an application of the original CSDS model to different types of interfaces with infills. Validation of the updated model should be carried out to showcase the applicability of the model to varying types of interfaces, and also address conditions of interests such as rock-concrete interfaces (see also work by Renaud et al. (2019)).

The model currently presents limitation in regards to its numerical formulation which cannot be readily implemented in a

Table 6
Rock properties used in this study. The data are taken from Khosravi (2016).

Sample	σ_3 (MPa)	B (°)	E (GPa)	σ_T (MPa)	S_o (MPa)	φ_0 (°)	i_0 (°)
BAS-29	24	17	45.4	280	33	53	33

Table 7
Direct shear results of BAS-29 from Khosravi and Simon (2018) at three normal stresses.

σ_n (MPa)	u_p (mm)	u_r (mm)	τ_p (MPa)	τ_r (MPa)	φ_u (°)	φ_r (°)
3	0.4	5.5	4	2.2	48	46
5	0.39	6	6.3	3.5		
8	0.44	6	9.9	6.9		

Table 8
Model properties obtained in this study by the application of the updated CSDS model.

σ_n (MPa)	u_p (mm)	u_r (mm)	τ_p (MPa)	τ_r (MPa)	φ_u (°)	φ_r (°)
3	0.51	5.9	3.5	2.2	46.6	43.5
5	0.51	6.7	5.8	3.54		
8	0.5	6	8.9	6.8		

numerical code. Future work shall be conducted to adapt the model formulation as a set of partial differential equations (PDE) considering computing cycles/steps. In its current form, the model does not account for strain rate or loading rate, which would leave unknown elements to a complete PDE formulation of the model. Simon (1999) proposed an incremental version of the original model for numerical applications which incorporated assumptions pertaining to the range of displacement rates applicable to the model. Further investigation and laboratory tests should be carried out to refine this aspect and clarify the relationship between strain rate and model response.

Table 9
The model parameters obtained in this study by using the modified CSDS method without direct shear test data.

σ_n (MPa)	u_p (mm)	u_r (mm)	τ_p (MPa)	τ_r (MPa)	φ_u (°)	φ_r (°)
3	0.51	6.5	4	2.7	53	42
5	0.51	5.4	5.8	4.5		
8	0.5	5.5	10.7	7.2		

Table 10
Rock properties taken from Ohnishi et al. (1993) and the model parameters obtained in this study.

σ_n (MPa)	JCS (MPa)	ϕ_b (°)	u_p (mm)	τ_p (MPa)	τ_r (MPa)	u_r (mm)	ϕ_r (°)	JRC_P	K_{ni} (MPa/mm)	V_m (mm)
2	50	33	1.35	2.86	1.59	25	33	15.7	1	0.41

Despite advantage of the modified model in incorporating mobilized roughness into the updated method for the predictions of shear stress and normal displacement, the scale effect on this factor was not considered. It is generally acknowledged that the shear behavior and deformability of rock joints are affected by scale. Numerous researchers (e.g. Miller, 1965; Pratt, 1974; Rengers, 1970; Barton and Choubey, 1977; Bandis et al., 1981; Yoshinaka et al., 1993; Ohnishi et al., 1993; Fardin, 2008; Bahaaddini, 2017; Tan et al., 2019; Deiminiat et al., 2022) have investigated the scale effect on the peak shear stress. Meanwhile, Deng and his colleagues studied the scale effect on the post-peak shear behavior of rock joints for the first time in 2004. They investigated the impact of scale on joint behavior based on the measurement of initial asperity angle of joint surfaces in the CSDS model, whereas the mobilized roughness upon shearing of joints of different lengths appear to be responsible for the scale effect in rock joints (Bandis, 1990). Since the CSDS model uses the initial asperity angle in calculations of shear behavior and normal displacement, it does not take into

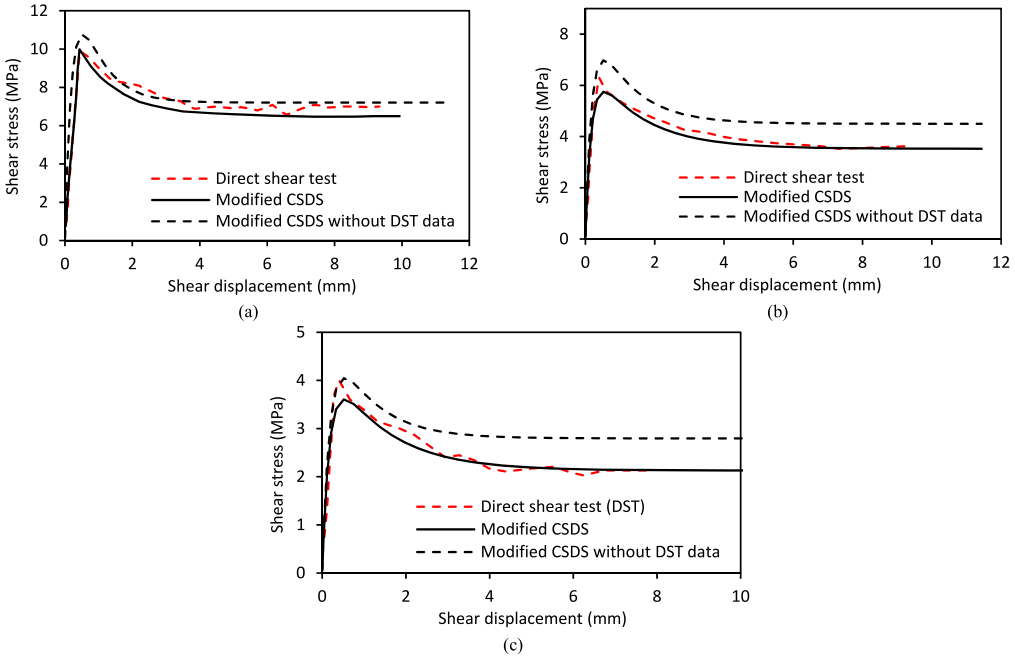

Fig. 6. Comparisons between full shear stress–displacement curves obtained by direct shear tests (DST) and those predicted by the modified CSDS model with and without DST. The experimental data are taken from Khosravi and Simon (2018) for normal loads of (a) 8 MPa, (b) 5 MPa and (c) 3 MPa.

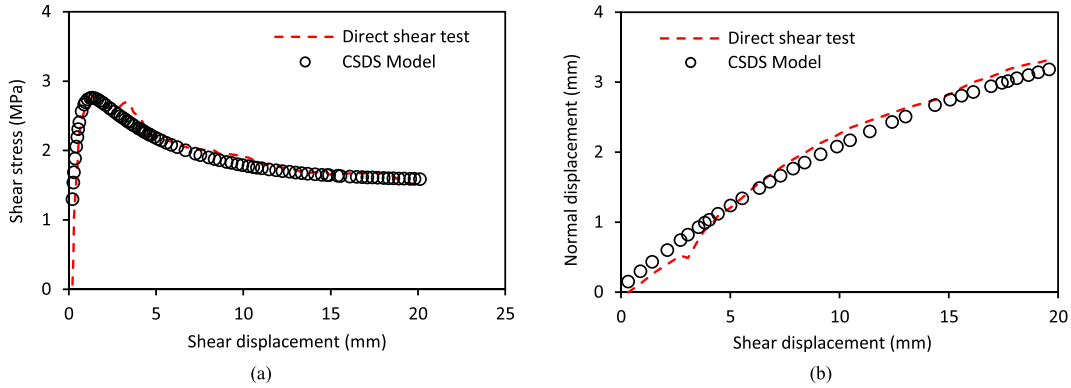

Fig. 7. Validation of the model for (a) shear stress–displacement and (b) normal-shear displacement curves of cement mortar with irregular surface. The direct shear test data are taken from Ohnishi et al. (1993).

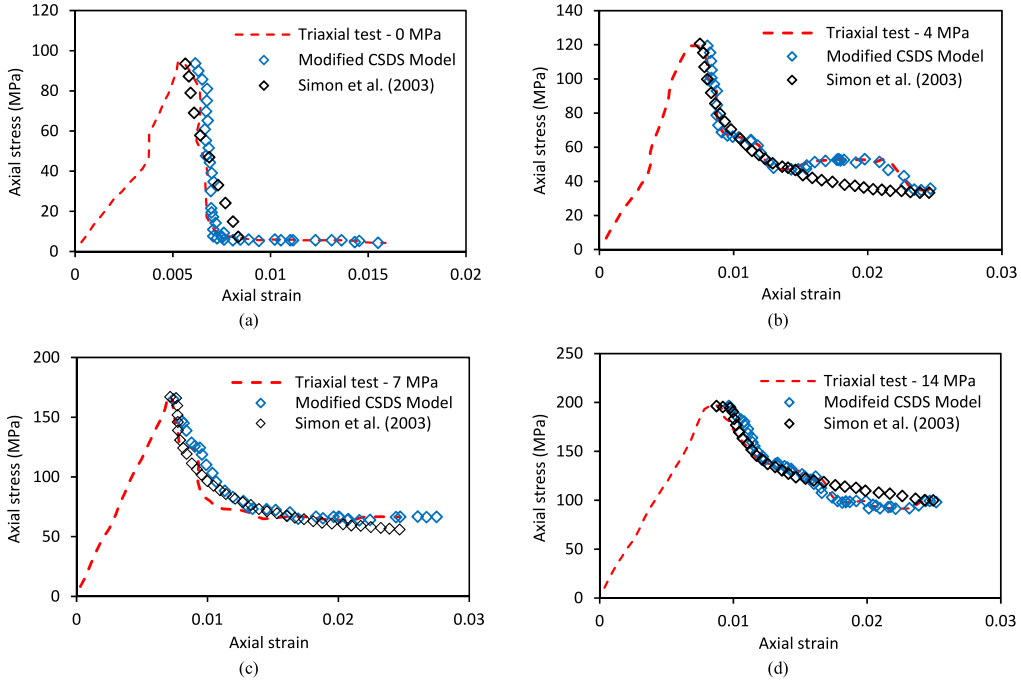

Fig. 8. Comparisons between the post-peak axial stress–strain curves obtained by this study and Simon et al. (2003) with the experimental curves taken from Price (1979) for confining pressures of (a) 0 MPa, (b) 4 MPa, (c) 7 MPa, and (d) 14 MPa.

account the influence of scale on ongoing deformation during shear and after peak.

However, incorporating the mobilizing *JRC* and Barton model into the updated model is intended to pave the way for topographical measurements (e.g. LiDAR scanners) and post-processing calibration of the model. Remote sensing topographical data of natural rock joints may be used to find a correlation between the roughness properties of small and natural rock joints. Select researchers have developed peak shear strength models that directly correlate peak shear strength to rock joint properties in a 3D effective area (e.g. Grasselli and Egger, 2003; Tatone and Grasselli, 2010; Tang and Wong, 2016; Yang et al., 2016; Liu et al., 2017; Magsipoc et al., 2020; Huang et al., 2022). Due to the requirement of these models for direct measurement of change in roughness with respect to shear plane direction, they have not been considered in this work. Instead, Barton model is used so that scale-free roughness could be easily included into prediction of shear strength and normal displacement in future works. Using the scale-dependent roughness coefficient in the estimation of shear behavior offers a novel opportunity to describe the post-peak and full shear behavior of large rock joints without scale effect using the updated CSDS model.

8. Conclusions

The following conclusions and observations are drawn from this work and results presented:

(1) It is crucial to consider the mobilized joint roughness coefficient (JRC_m) in the estimation of post-peak shear behavior. It could also be seen from the comparison shown in Fig. 2.
(2) The updated model well describes the post-peak and complete axial stress–strain curves with the use of triaxial compression test data.

Table 11
Rock properties and CSDS model properties obtained by Khosravi (2016) for basalt (BAS) and microgabbro (MG).

Sample	σ_3 (MPa)	B (°)	E^a (GPa)	u_p (mm)	u_r (mm)	K_{ni} (MPa/mm)	V_m (mm)	$\sigma_T{}^a$ (MPa)	$S_o{}^a$ (MPa)	$\varphi_0{}^a$ (°)	φ_r (°)	i_0 (°)
BAS-23	20	22	45.4	0.005	3	N/A	N/A	280	33	53	46	33
BAS-29	24	17	45.4	0.005	3	N/A	N/A	280	33	53	46	33
MG-17	24	24	39	0.005	2.5	N/A	N/A	180	27	48	41	25
MG-19	15	25.5	39	0.005	2.5	N/A	N/A	180	27	52	46	28

[a] Rock properties.

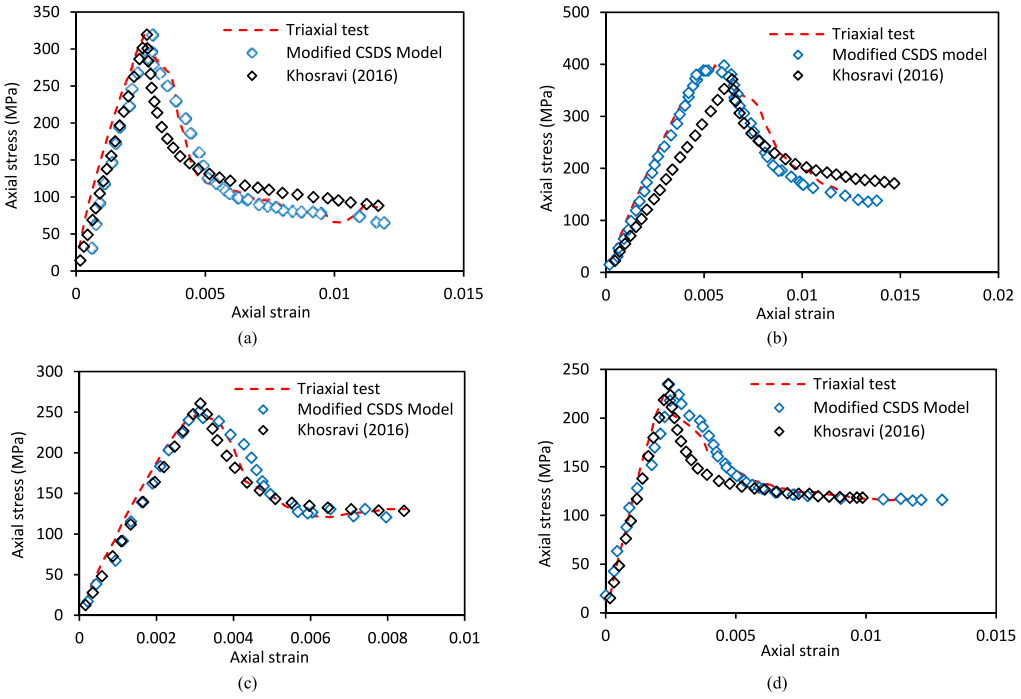

Fig. 9. Comparisons of full axial stress–strain curves obtained by this study and Khosravi (2016) for (a) BAS-23, (b) BAS-29, (c) MG-17, and (d) MG-19 with the experimental curves taken from Khosravi (2016).

Table 12
Rock properties taken from Arzúa and Alejano (2013), and model properties obtained in this study.

σ_3 (MPa)	B (°)	E^a (GPa)	u_p (mm)	u_r (mm)	JRC	K_{ni} (MPa/mm)	V_m (mm)	$\sigma_T{}^a$ (MPa)	$S_o{}^a$ (MPa)	$\varphi_0{}^a$ (°)	φ_r (°)	i_0 (°)
4	24.3	22.61	0.045	2.53	31	48.9	0.39	57.8	8	46	52.4	38.7
12	14.2	48.84	0.07	2.5	38.2	63.1	0.26	126.7	16.8	46	48.5	49.5

[a] Rock properties.

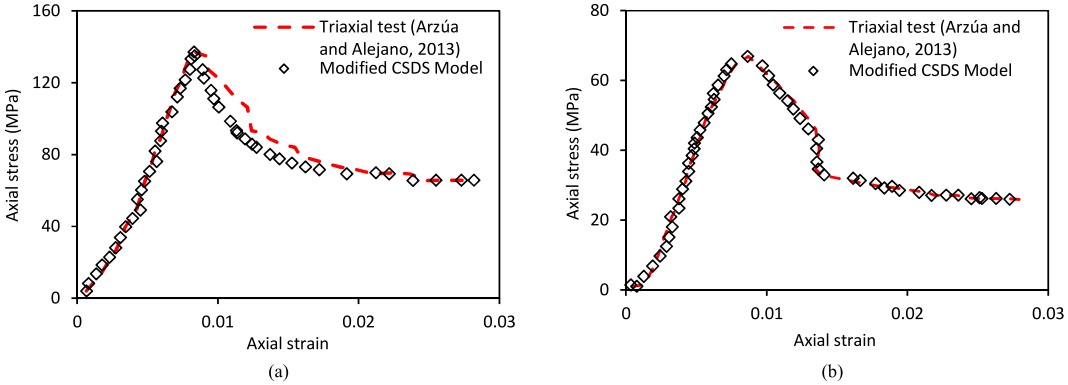

Fig. 10. Comparison of the full stress–strain curves obtained by the modified model with the experimental curves reported by Arzúa and Alejano (2013) for (a) $\sigma_3 = 4$ MPa and (b) $\sigma_3 = 12$ MPa.

(3) Available and updated versions of CSDS model could predict the post-peak shear stress–displacement curves with the use of triaxial compression test results. These curves, however, do not correspond to those obtained by direct shear test results.
(4) The updated model accurately obtains the complete shear stress–displacement curves. A requirement for making accurate prediction is to use direct shear test data for the estimate of model parameters *a*, *b*, *c*, *d* and *e*.
(5) In the absence of direct shear test data, the alternative method proposed in this work may be used to determine model properties for the prediction of full shear stress–displacement profiles. Nevertheless, more works on the validation of this method can be necessary with using the experimental data of different materials obtained under different normal loads.

Declaration of competing interest

The authors declare that they have no known competing financial interests or personal relationships that could have appeared to influence the work reported in this paper.

Acknowledgments

The authors acknowledge the financial support from Natural Sciences and Engineering Research Council of Canada through its Discovery Grant program (RGPIN-2022-03893), and École de Technologie Supérieure (ÉTS) construction engineering research funding. Special thanks to Richard Simon and Khosravi for the data sets provided and the positive feedback pertaining to this work.

References

Amadei, B., Saeb, S., 1990. Constitutive models of rock joints. In: Barton, N., Stephansson, O. (Eds.), Rock Joints- Proceedings of an International Symposium on Rock Joints. A.A. Balkema, Rotterdam, Netherlands, pp. 581–594.
Arzúa, J., Alejano, L.R., 2013. Dilation in granite during servo-controlled triaxial strength tests. Int. J. Rock Mech. Min. Sci. 61, 43–56.
Asadollahi, P., 2009. Stability Analysis of a Single Three-Dimensional Rock Block: Effect of Dilatancy and High-Velocity Water Jet Impact. PhD Thesis. University of Texas at Austin, Austin, Texas, USA.
Asadollahi, P., Tonon, F., 2010. Constitutive model for rock fractures: revisiting Barton's empirical model. Eng. Geol. 113 (1–4), 11–32.
ASTM D5607-16, 2016. Standard Test Method for Performing Laboratory Direct Shear Strength Tests of Rock Specimens under Constant Normal Force. ASTM International, West Conshohocken, PA, USA.
ASTM D2664-04, 2004. Standard Test Method for Triaxial Compressive Strength of Undrained Rock Core Specimens without Pore Pressure Measurements. ASTM International, West Conshohocken, PA, USA.
ASTM D7012-23, 2023. Standard Test Methods for Compressive Strength and Elastic Moduli of Intact Rock Core Specimens under Varying States of Stress and Temperatures. ASTM International, West Conshohocken, PA, USA.
Aubertin, M., Julien, M., Li, L., 1998. The semi-brittle behavior of low porosity rocks. In: Rock Machanics – Proceedings of the 3rd North American Rock Mechanics Symposium (NARMS'98). Pergamon, Cancun, Mexico, pp. 65–90.
Bahaaddini, M., 2017. Effect of boundary condition on the shear behaviour of rock joints in the direct shear test. Rock Mech. Rock Eng. 50 (5), 1141–1155.
Bandis, S., 1980. Experimental Studies of Scale Effects on Shear Strength, and Deformation of Rock Joints. PhD Thesis. University of Leeds, Leeds, UK.
Bandis, S., Lumsden, A.C., Barton, N.R., 1981. Experimental studies of scale effects on the shear behaviour of rock joints. Int. J. Rock Mech. Min. Sci. Geomech. Abstr. 18 (1), 1–21.
Bandis, S.C., Lumsden, A.C., Barton, N.R., 1983. Fundamentals of rock joint deformation. Int. J. Rock Mech. Min. Sci. Geomech. Abstr. 20 (6), 249–268.
Bandis, S.C., 1990. Scale effects in the strength and deformability of rocks and rock joints. In: Pinto de Cunha, A. (Ed.), Scale Effects in Rock Masses: Proceedings of the 1st International Workshop on Scale Effects in Rock Masses. A.A. Balkema, Rotterdam, Netherlands, pp. 59–76.
Barton, N., 1973. Review of a new shear-strength criterion for rock joints. Eng. Geol. 7 (4), 287–332.
Barton, N., Choubey, V., 1977. The shear strength of rock joints in theory and practice. Rock Mech. 10 (1), 1–54.
Barton, N., 1982. Modelling Rock Joint Behavior from in Situ Block Tests: Implications for Nuclear Waste Repository Design. Office of Nuclear Waste Isolation, Battelle Project Management Division, Columbus, Ohio, US, p. 96.
Barton, N., 2013. Shear strength criteria for rock, rock joints, rockfill and rock masses: problems and some solutions. J. Rock Mech. Geotech. Eng. 5 (4), 249–261.
Day, J.J., Diederichs, M.S., Hutchinson, D.J., 2017a. New direct shear testing protocols and analyses for fractures and healed intrablock rockmass discontinuities. Eng. Geol. 229, 53–72.
Day, J.J., Diederichs, M.S., Hutchinson, D.J., 2017b. The influence of mineralogy and grain scale features in healed intrablock rockmass structure on direct shear properties in the Cobourg limestone. In: 51st US Rock Mechanics Geomechanics Symposium. ARMA, Minneapolis, USA.
Deiminiat, A., Li, L., Zeng, F., 2022. Experimental study on the minimum required specimen width to maximum particle size ratio in direct shear tests. Civ. Eng. 3 (1), 66–84.
Deng, D., Simon, R., Aubertin, M., 2004. A geometrical approach for the estimation of scale effects in rock joint behaviour. In: Proceedings of the 57th Canadian Geotechnical Conference and Joint CGS - IAH Groundwater Specialty Conference: Geoengineering for the Society and Environment. BiTech, Quebec City, QC, Canada, pp. 33–40.
Deng, D., Simon, R., Aubertin, M., 2006. Modelling shear and normal behaviour of filled rock joints. In: DeGroot, D.J., DeJong, J.T., Frost, D., Baise, L.G. (Eds.), GeoCongress 2006: Geotechnical Engineering in the Information Technology Age. ASCE Press, Atlanta, Georgia, USA, pp. 1–6.
Eberhardt, E., Stead, D., Stimpson, B., Read, R.S., 1998. Identifying crack initiation and propagation thresholds in brittle rock. Can. Geotech. J. 35 (2), 222–233.
Fairhurst, C., Hudson, J., 1999. Draft ISRM suggested method for the complete stress-strain curve for intact rock in uniaxial compression. Int. J. Rock Mech. Min. Sci. 36 (3), 279–289.
Fardin, N., Stephansson, O., Jing, L., 2001. The scale dependence of rock joint surface roughness. Int. J. Rock Mech. Min. Sci. 38 (5), 659–669.
Fardin, N., Feng, Q., Stephansson, O., 2004. Application of a new in situ 3D laser scanner to study the scale effect on the rock joint surface roughness. Int. J. Rock Mech. Min. Sci. 41 (2), 329–335.
Fardin, N., 2008. Influence of structural non-stationarity of surface roughness on morphological characterization and mechanical deformation of rock joints. Rock Mech. Rock Eng. 41 (2), 267–297.
Fortin, M., Archambault, G., Aubertin, M., Gill, D.E., 1988. An algorithm for predicting the effect of a variable normal stiffness on shear strength of discontinuities. In: Proceedings of the 15th Canadian Rock Mechanic Symposium. CARMA, Toronto, ON, Canada, pp. 109–117.
Fotoohi, K., 1993. Nonlinear Boundary Element Analysis of a Rock Mass with Discontinuities. PhD Thesis. McGill University, Montréal, QC, Canada.
Franklin, J.A., Kanji, M.A., Herget, G., et al., 1974. Suggested methods for determining shear strength. Int. J. Rock Mech. Min. Sci. Geomech. Abstr. (1), 131–140.
Goodman, R.E., Taylor, R.L., Brekke, T.L., 1968. A model for the mechanics of jointed rock. J. Soil Mech. Found Div. 94 (3), 637–659.
Goodman, R.E., 1976. Methods of Geological Engineering in Discontinuous Rocks. West Group, St-Paul, MN, USA.
Goodman, R.E., St John, C., 1977. Finite element analysis for discontinuous rocks. In: Desai, C.S., Christian, J.t. (Eds.), Numerical Methods in Geotechnical Engineering. McGraw-Hill, University of California, CA, USA, pp. 148–175.
Goodman, R.E., 1980. Introduction to Rock Mechanics, second ed. John Wiley & Sons, New York, USA.
Grasselli, G., 2001. Shear Strength of Rock Joints Based on Quantified Surface Description. PhD Thesis. EPFL, Lausanne, Switzerland.
Grasselli, G.I., Wirth, J., Egger, P., 2002. Quantitative three-dimensional description of a rough surface and parameter evolution with shearing. Int. J. Rock Mech. Min. Sci. 39 (6), 789–800.
Grasselli, G., Egger, P., 2003. Constitutive law for the shear strength of rock joints based on three-dimensional surface parameters. Int. J. Rock Mech. Min. Sci. 40 (1), 25–40.
Haberfield, C.M., Johnston, I.W., 1994. A mechanistically-based model for rough rock joints. Int. J. Rock Mech. Min. Sci. Geomech. Abstr. 31 (4), 279–292.
Homand, F., Belem, T., Souley, M., 2001. Friction and degradation of rock joint surfaces under shear loads. Int. J. Numer. Anal. Methods GeoMech. 25 (10), 973–999.
Huang, X., Haimson, B.C., Plesha, M.E., Qiu, X., 1993. An investigation of the mechanics of rock joints—Part I. Laboratory investigation. Int. J. Rock Mech. Min. Sci. Geomech. Abstr. 30 (3), 257–269.
Huang, M., Hong, C., Sha, P., Du, S., Luo, Z., Tao, Z., 2022. Method for visualizing the shear process of rock joints using 3D laser scanning and 3D printing techniques. J. Rock Mech. Geotech. Eng. 15 (1), 204–215.
ISRM, 1978. Suggested methods for the quantitative description of discontinuities in rock masses. Int. J. Rock Mech. Min. Sci. Geomech. Abstr. 15, 319–368.
ISRM, 1989. Suggestion method for large scale sampling and triaxial testing of joined rock. Int. J. Rock Mech. Min. Sci. Geomech. Abstr. 26 (5), 427–434.
Jang, B.A., Jang, H.S., Park, H.J., 2006. A new method for determination of joint roughness coefficient. In: Culshaw, M.G., Reeves, H.J. (Eds.), 10th Congress of the International Association for Engineering Geology and the Environment (IAEG 2006). Geological Society, London, UK.
Khosravi, A., 2016. Estimation and Validation of Post-peak Behavior of Hard Rocks. PhD Thesis. Ecole Polytechnique, Montréal, QC, Canada.

Khosravi, A., Simon, R., 2018. Verification of the CSDS model in estimating the postpeak behavior of hard rocks. Int. J. GeoMech. 18 (3), 04017166.
Kim, D.Y., Lee, H.S., Kulatilake, P.H.S.W., 2009. Quantification of rock joint roughness and development of analyzing system. In: Kulatilake, P.H.S.W. (Ed.), Proceedings of the International Conference on Rock Joints and Jointed Rock Masses, pp. 7–8. Tucson.
Ladanyi, B., Archambault, G., 1969. Simulation of shear behavior of a jointed rock mass. In: The 11th U.S. Symposium on Rock Mechanics (USRMS1969). American Rock Mechanics Association (ARMA), Berkeley, CA, USA, pp. 105–125.
Lee, Y.H., Carr, J.R., Barr, D.J., Haas, C.J., 1990. The fractal dimension as a measure of the roughness of rock discontinuity profiles. Int. J. Rock Mech. Min. Sci. Geomech. Abstr. 27 (6), 453–464.
Li, Y., Yang, H., Sun, S., 2022. Unveiling the mystery of scale dependence of surface roughness of natural rock joints. Sci. Rep. 12 (1), 1–15.
Li, L., Gamache, M., Aubertin, M., 2000. Parameter determination for nonlinear stress criteria using a simple regression tool. Can. Geotech. J. 37 (6), 1332–1347.
Liu, Q., Tian, Y., Liu, D., Jiang, Y., 2017. Updates to JRC-JCS model for estimating the peak shear strength of rock joints based on quantified surface description. Eng. Geol. 228, 282–300.
Magsipoc, E., Zhao, Q., Grasselli, G., 2020. 2D and 3D roughness characterization. Rock Mech. Rock Eng. 53, 1495–1519.
Martin, C.D., 1993. Strength of massive Lac du Bonnet granite around underground openings. PhD Thesis. University of Manitoba, Winnipeg, Manitoba, Canada.
Martin, C.D., Chandler, N.A., 1994. The progressive fracture of Lac du Bonnet granite. Int. J. Rock Mech. Min. Sci. Geomech. Abstr. 31 (6), 643–659.
Miller, R.P., 1965. Engineering Classification and Index Properties for Intact Rock. PhD Thesis. University of Illinois, Champaign, IL, USA.
Niktabar, S.M., Rao, K.S., Shrivastava, A.K., 2017. Effect of rock joint roughness on its cyclic shear behavior. J. Rock Mech. Geotech. Eng. 9 (6), 1071–1084.
Ohnishi, Y., Herda, H., Yoshinaka, R., 1993. Shear strength scale effect and the geometry of single and repeated rock joints. In: Pinto de Cunha, A. (Ed.), In Scale Effects in Rock Masses 93, first ed. Taylor & Francis Group, CRC Press, London. UK, pp. 167–173.
Packulak, T.R., Day, J.J., Diederichs, M.S., 2018. Assess: the Role of Rock Direct Shear Testing in Determining Geomechanical Properties of Fractures. Tunnels and Tunnelling. Tunneling Association of Canada, Canada, pp. 32–36.
Packulak, T.R., Day, J.J., Diederichs, M.S., 2022a. Enhancement of constant normal stiffness direct shear testing protocols for determining geomechanical properties of fractures. Can. Geotech. J. 59 (9), 1643–1659.
Packulak, T.R., Day, J.J., Ahmed Labeid, M.T., Diederichs, M.S., 2022b. New data processing protocols to isolate fracture deformations to measure normal and shear joint stiffness. Rock Mech. Rock Eng. 55 (5), 2631–2650.
Patton, F.D., 1966. Multiple Modes of Shear Failure in Rock and Related Materials. PhD Thesis. University of Illinois, Champaign, IL, USA.
Pratt, H.R., 1974. Friction and deformation of jointed quartz diorite. In: Proceeding of the 3rd International Society for Rock Mechanics and Rock Engineering Congress. ISRM), Denver, USA, pp. 306–310.
Price, A.M., 1979. The Effects of Confining Pressure on the Post-yield Deformation Characteristics of Rocks. PhD Thesis. Newcastle University, Newcastle upon Tyne, England.
Renaud, S., Saichi, T., Bouaanani, N., Miquel, B., Quirion, M., Rivard, P., 2019. Roughness effects on the shear strength of concrete and rock joints in dams based on experimental data. Rock Mech. Rock Eng. 52, 3867–3888.
Rengers, N., 1970. Influence of surface roughness on the friction properties of rock planes. Proceedings of International Society of Rock Mechanics 1 (1–31), 229–234.
Saeb, S., Amadei, B., 1992. Modelling rock joints under shear and normal loading. Int. J. Rock Mech. Min. Sci. Geomech. Abstr. 29, 267–278.
Sanei, M., Faramarzi, L., Fahimifar, A., Goli, S., Mehinrad, A., Rahmati, A., 2015a. Shear strength of discontinuities in sedimentary rock masses based on direct shear tests. Int. J. Rock Mech. Min. Sci. 75, 119–131.
Sanei, M., Faramarzi, L., Goli, S., Fahimifar, A., Rahmati, A., Mehinrad, A., 2015b. Development of a new equation for joint roughness coefficient (JRC) with fractal dimension: a case study of Bakhtiary Dam site in Iran. Arabian J. Geosci. 8 (1), 465–475.
Simon, R., 1999. Analysis of Fault-Slip Mechanisms in Hard Rock Mining. PhD Thesis. McGill University, Montreal, QC, Canada.
Simon, R., Aubertin, M., Deng, D., 2003. Estimation of post-peak behaviour of brittle rocks using a constitutive model for rock joints. In: 56th Canadian Geotechnic Conference. Canadian Geotechnical Society (CGS), Winnipeg, Manitoba, Canada.
Tan, R., Chai, J., Cao, C., 2019. Experimental investigation of the permeability measurement of radial flow through a single rough fracture under shearing action. Adv. Civ. Eng. 2019, 6717295.
Tang, Z.C., Wong, L.N.Y., 2016. New criterion for evaluating the peak shear strength of rock joints under different contact states. Rock Mech. Rock Eng. 49 (4), 1191–1199.
Tang, Z.C., Zhang, Z.F., Zuo, C.Q., Jiao, Y.Y., 2021. Peak shear strength criterion for mismatched rock joints: revisiting JRC-JMC criterion. Int. J. Rock Mech. Min. Sci. 147, 104894.
Tatone, B.S., Grasselli, G., 2010. A new 2D discontinuity roughness parameter and its correlation with JRC. Int. J. Rock Mech. Min. Sci. 47 (8), 1391–1400.
Thirukumaran, S., Indraratna, B., 2016. A review of shear strength models for rock joints subjected to constant normal stiffness. J. Rock Mech. Geotech. Eng. 8 (3), 405–414.
Tian, Y., Liu, Q., Ma, H., Liu, Q., Deng, P., 2018. New peak shear strength model for cement filled rock joints. Eng. Geol. 233, 269–280.
Tremblay, D., 2005. Une analyse numérique du comportement hydromécanique des discontinuités en massif rocheux fracturé. Master Thesis. Polytechnique Montréal, Montréal, QC, Canada.
Tremblay, D., Simon, R., Aubertin, M., 2007. A constitutive model to predict the hydromechanical behavior of rock joints. In: Proceedings of the 60th Canadian Geotechnical Conference and 8th Joint CGS/IAH-CNC Groundwater Conference (GeoOttawa 2007). Canadian Geotechnical Society, Ottawa, ON, Canada, pp. 2011–2018.
Wang, F., Wang, S., Yao, W., Li, X., Meng, F., Xia, K., 2022. Effect of roughness on the shear behavior of rock joints subjected to impact loading. J. Rock Mech. Geotech. Eng. 2022.
Xia, C.C., Tang, Z.C., Xiao, W.M., Song, Y.L., 2014. New peak shear strength criterion of rock joints based on quantified surface description. Rock Mech. Rock Eng. 47 (2), 387–400.
Yang, Z.Y., Di, C.C., Yen, K.C., 2001. The effect of asperity order on the roughness of rock joints. Int. J. Rock Mech. Min. Sci. 38 (5), 745–752.
Yang, J., Rong, G., Hou, D., Peng, J., Zhou, C., 2016. Experimental study on peak shear strength criterion for rock joints. Rock Mech. Rock Eng. 49 (3), 821–835.
Yoshinaka, R., Yoshida, J., Arai, H., Arisaka, S., 1993. Scale effects on shear strength and deformability of rock joints. In: Pinto de Cunha, A. (Ed.), In Scale Effects in Rock Masses 93, first ed. Taylor & Francis Group, CRC Press, London. UK, pp. 143–149.
Zhang, G., Karakus, M., Tang, H., Ge, Y., Zhang, L., 2014. A new method estimating the 2D joint roughness coefficient for discontinuity surfaces in rock masses. Int. J. Rock Mech. Min. Sci. 72, 191–198.
Zheng, B., Qi, S., 2016. A new index to describe joint roughness coefficient (JRC) under cyclic shear. Eng. Geol. 212, 72–85.

Akram Deiminiat obtained a Master degree of Civil Engineering from University of Urmia. She subsequently worked 6 years as a hydro-geo-technique engineer and project manager for a consulting firm in Iran. In 2017, she immigrated to Canada to pursue a PhD in Mining Engineering at Polytechnique Montréal, completing her thesis in 2022. Her research work led to the revision of ASTM experimental methods for specimen size requirements in direct shear tests, and the publication of four peer-reviewed journal papers. Dr. Deiminiat now works as a post-doctoral researcher at École de Technologie Supérieure (ÉTS) in Montréal, Canada. Her current research focus includes experimental investigations on the mechanical behaviors and shear stress of granular materials and rock joints for slope stability problems; and (2) theoretical study and numerical modeling of constitutive shear models with respect to time. Dr. Deiminiat has co-authored over 15 research publications and taken part in a number of technical symposia and international conferences.